



ORIGINAL RESEARCH ARTICLE

Mechanically Alloyed FeNi and Fe Powders Crystalline Size, Phase Formation, and Morphology: Investigation on Milling Time Impact

Naouaem Boudinar, Sofiane Chiheb , Nawel Nedjah, Nour Elhouda Arabi, Abdelmalik Djekoun, and Bouguerra Bouzabata

Submitted: 22 December 2023 / Revised: 24 June 2024 / Accepted: 30 June 2024

The present paper is devoted to study the structural, morphological, and magnetic behavior of Fe₅₀Ni₅₀ alloy and pure Fe powder prepared by mechanical alloying. The powder has been milled with high-energy ball milling process with 24 h and 32 h for FeNi and Fe powders, respectively. The x-ray diffraction, scanning electron microscopy, Mössbauer spectroscopy, and vibrating sample magnetometer techniques have been employed to identify the characteristics of the milled powders. The first x-ray diffraction results show that increasing milling time for pure Fe exhibits bcc-type reflections, with rapid decrease in crystallite size and a slight increase in lattice, and no other phase appears during milling, while for Fe₅₀Ni₅₀ alloy, fcc phase appears after 8 h of milling with disappearance of Fe peaks. SEM and FE-SEM results have shown morphological changes are appearing in the structures where crystallite size for Fe₅₀Ni₅₀ is 33.49 nm and the one for pure Fe is 15 nm. Mössbauer spectroscopy proved that during the mechanical alloying process, the hyperfine field of Fe₅₀Ni₅₀ decreases from 33 to 32 T, 31, and 29 T, respectively after 2, 8, and 24 h of milling. For the FeNi alloy, Vibrating Sample Magnetometer (VSM) at room temperature has been used, and the Hysteresis cycles has been plotted for several times of milling. The magnetic coercivity increased and the saturation magnetization decreased after the first two hours due to the morphological changes in particles leading to considerable changes in remanent magnetization and squareness ratio. These changes have disappeared during milling operations where particles sizes become equal. During FeNi milling, morphological changes lead to change the Hysteresis loops after 2 h of milling. At the end of milling, a remanent magnetization of 0.118 emu and coercivity of 32.85 G have been noted. The magnetic moment in Bohr magnetron for the alloy is 0.1338.

Keywords magnetic property, mechanical alloying, Mössbauer spectroscopy, scanning electron microscopy, x-ray diffraction

1. Introduction

The nanostructured magnetic materials have become attractive for a wide range of applications in various fields, such as electronics, medicine, and energy. Compared to micrometric materials, they are characterized by improved mechanical, optical, and electrical properties, with enhancing chemical

reactivity, and material consumption for production is reduced. A wide variety of techniques have been used to synthesize nanostructured metallic materials including inert gas condensation (Ref 1, 2), electrodeposition (Ref 3, 4), crystallization of amorphous phases (Ref 5, 6), sputtering (Ref 7, 8), or mechanical alloying (Ref 9, 10). The nanomaterials are used in other fields like coating (Ref 11) and dislocation motion study (Ref 12).

Mechanical Alloying (MA) is an alternative technique used to produce new materials, to obtain metastable materials or to modify the properties of existing ones. It is a complex process involving deformation, fragmentation, cold solder, and microdiffusion in a highly energetic grinding media, by applying repeated cold welding, fracturing, and re-welding of powder of different compositions in a high-energy ball mill or similar equipment. In the end, a solid-state powder is obtained. The MA is used widely in Materials Science (studying the properties), powder metallurgy (producing high-performance powder, hot isostatic pressing), catalysis, energy storage (electrode materials production), and for biomedical engineering (producing biocompatible materials) (Ref 13, 14). The Fe powder is widely used in metallurgy processes where the metal density can be controlled, while the FeNi alloy is used in transformers and inductors of high-frequency applications.

Zhang and Zhitomirsky (Ref 15) have investigated the mechanical alloying for ferrimagnetic materials using high-energy ball milling. The obtained results show that the use of the ferrimagnetic composites is promising for the fabrication of

Naouaem Boudinar, National Higher School of Technology and Engineering ENSTI, Laboratoire de Technologies des Systemes Energetiques LTSE, 23005 Annaba, Algeria; and Laboratoire de Magnetisme et de Spectroscopie des Solides, Universite Badji Mokhtar, Faculte des sciences, BP12 Sidi Amar, 23000 Annaba, Algeria; **Sofiane Chiheb**, **Nawel Nedjah**, and **Nour Elhouda Arabi**, National Higher School of Technology and Engineering ENSTI, Laboratoire de Technologies des Systemes Energetiques LTSE, 23005 Annaba, Algeria; **Abdelmalik Djekoun** and **Bouguerra Bouzabata**, Laboratoire de Magnetisme et de Spectroscopie des Solides, Universite Badji Mokhtar, Faculte des sciences, BP12 Sidi Amar, 23000 Annaba, Algeria. Contact e-mails: n.boudinar@ensti-annaba.dz and s.chiheb@ensti-annaba.dz.

the devices based on mutual interaction. Lui et al. (Ref 16) have studied an alloy composed of Fe, Se, and Te where the phase transition mechanism produced by high-energy ball milling was accompanied by sintering method. The obtained results show that used production methods can decrease the superconducting phase formation temperature and enhance the fabrication efficiency.

Many investigations have studied the nanomaterials alloys based on Fe: Kurichenko et al. (Ref 17) have studied FeNi nanopowder using cycling oxidation and reduction with temperature of 320 °C. The results show that oxidation and reduction do not affect the FeNi presence in the powder using differential scanning calorimetry analysis and magnetic measurements. Ferrimagnetic behavior of magnetic FeM ($M_{1/4}Ag, Co, Cu, \text{ and } Ni$) nanocrystals has been studied by Freire et al. (Ref 18). Panigrahi and Avar (Ref 19) have studied the impact of mechanical alloying composed of $Fe_{50}Ni_{10}Co_{10}Ti_{10}B_{20}$ until 50 h and under argon gas. The results have shown the appearance of amorphous phase after 20 h of milling. At the end of alloying, the obtained saturation magnetization was 89.7 emu/g and the coercivity was 32.5 Oe. The nanocrystals studied are structured in body-centered cubic (bcc) unit cell and in a face-centered cubic (fcc) one. The nanocrystals have been analyzed using x-ray diffraction, transmission electron microscopy, and Mössbauer analyses. The obtained results show that the studied materials are sustainable for electrochemical water splitting. Many alloys based on Ni have been studied in recent works, like the morphological study of NiTi alloy when exposed to electromagnetic pulse welding (Ref 20), and the results reported that the alloy is influenced by strain rate and peak pressure appearing during welding. Long et al. (Ref 21) have studied nickel-based alloy under cyclic loading to investigate plastic deformation and damage-induced degradation. The results have shown that the internal regions of the studied alloy have been exposed to damages characterized by different evolutions.

For the FeNi alloy, many works have studied the characteristics of their alloys: Mushnikov et al. (Ref 22) have studied FeNi alloys with Ni concentration range of 0-20 %. The samples have been studied using x-ray diffraction and differential scanning calorimetry, with measuring of magnetic susceptibility. The results show that increasing Ni concentration leads to an expansion of the hysteresis of martensitic transformation. Sharma et al. (Ref 23) have investigated structural, magnetic, and magnetocaloric properties of the $Fe_{65}Ni_{35}$ alloy. The analysis is done using x-ray diffraction, zero-field-cooled cooling (ZFC), field-cooled cooling (FCC), and field-cooled warming (FCW). Below 88 °K, the first-order nature of the sample is observed, while the second-order nature is found near the magnetic ordering temperature, and the applied field-dependent confirms the non-saturated nature of the alloy.

Rodriguez et al. (Ref 24) have analyzed $Fe_{50}Ni_{50}$ prepared using high-energy milling method, and the analysis is done using x-ray diffraction pattern and Mössbauer spectroscopy. The results show that the extreme conditions of T-FeNi phase formation can be simulated with the used production method. In other work, Ref 25, nanostructured $(Fe_{0.5}Ni_{0.5})_{92}Zr_{5}B_3$ alloy has been prepared using high-energy milling and studied using the same techniques (x-ray diffraction pattern and Mössbauer spectroscopy). Rodriguez et al. have noticed that 30h-milled powdered material is a good material permitting the magnetic interaction study between atomically ordered phases, and to obtain finally a nanocomposite character. We note that

mechanical alloying is used in other alloys without incorporating Fe powder like cobalt monosilicide (CoSi) (Ref 26) and aluminum-boron carbide (Al-B₄C) (Ref 27). In precedent investigation (Ref 28), we have studied the $Fe_{50}Ni_{50}$ and $Fe_{64}Ni_{36}$ alloys formation using MA technique. The alloys have been studied using x-ray diffraction and scanning electron microscopy. The results show that the crystallite size of FeNi has been reduced to 14 nm, and the structure has been refined.

The novelty of this investigation is to explore the synthesis of nanomaterial powders—including pure Fe and $Fe_{50}Ni_{50}$ —through Mechanical Alloying (MA) via high-energy ball milling. Particularly, the $Fe_{50}Ni_{50}$ alloy exhibits a face-centered cubic crystal lattice structure, commonly referred to as “taenite.”

In addition to the characterization using x-ray Diffraction (XRD), Scanning Electron Microscopy (SEM) and Field Emission Scanning Electron Microscope (FE-SEM) were employed to observe powder morphology in the scale of micro- and nanometers. Furthermore, the size, phase analysis, and magnetic properties of taenite were investigated using Mössbauer Spectroscopy (MS). In the final step, Vibrating Sample Magnetometer (VSM) highlights many magnetic characteristics for milled FeNi nanostructured powder with various milling times. The VSM analysis permits to identify the FeNi saturation magnetization, coercivity, and squareness ratio of the $Fe_{50}Ni_{50}$ mechanical alloy, which—to the author’s knowledge—have not been presented before.

2. Experimental

Two compositions have been milled in SPEX 8000 M mixer/mill using three hardened steel balls (Fig. 1). The powdered Fe and Ni with particles are lower than 10 μm with purity of materials powders being 99.99 and 99.98 %, respectively. The milled compositions consist of 3 g of pure Fe powder and mixture of $Fe_{50}Ni_{50}$ with 3 g of each material powder. In order to minimize oxygen contamination, the vials were sealed under pure argon atmosphere and milled at room temperature. The used ball for milling weight is six times greater than powder one. The speed of ball milling of the tested samples was fixed at 1200 rpm.

The studied powder compositions have been milled at different times: The FeNi alloy has been milled from half an hour to 24 h, while the pure Fe powder has been milled until 32 h. For cooling system to both compositions, a pause of 15 min is taken after each 30 min of milling.

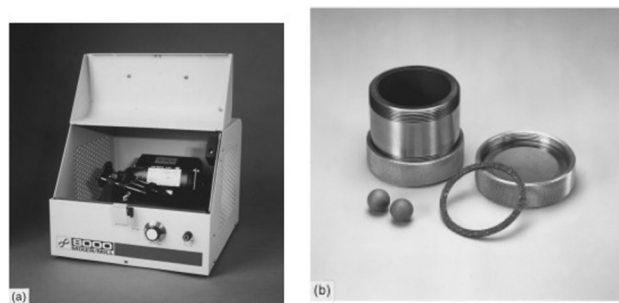


Fig. 1 SPEX 8000 M mixer/mill (Ref 29)

The samples are analyzed using a combination of non-destructive techniques:

1. The analysis of x-ray diffraction has been done using D501 Siemens diffractometer with a continuous scanning mode. The lamp used for Fe₅₀Ni₅₀ powder is of Cu – k_α radiation ($\lambda_{\alpha} = 1.54056\text{\AA}$), and the one used for Fe powder is of Co anticathode ($\lambda_{\alpha} = 1.78876\text{\AA}$). This analysis allows for the determination of the structural characterization and crystallite sizes. X-ray diffraction patterns were analyzed using the MAUD program based on the Rietveld method, combined with Fourier analysis (Ref 30, 31).
2. Scanning Electron Microscopy (SEM) and Field Emission Scanning Electron Microscope (FE-SEM) are valuable techniques which permit studying the microstructure, morphology, and particle size of the samples.
3. Conventional transmission Mössbauer spectroscopy is a valuable tool for studying the electronic, magnetic, and structural properties of FeNi alloys. It consists in measuring the energy of gamma rays emitted by a nucleus that has undergone a nuclear transition. Using a ⁵⁷Co source in rhodium matrix at room temperature and a metallic iron for calibration, the obtained spectra from Mössbauer were fitted using the MOSFIT program (Ref 32).
4. With a maximum applied magnetic field of 16 kOe, vibrating sample magnetometer has been used to study the magnetic properties of the samples. The global parameters of the experimental test done are presented in the next table (Table 1).

By using the above techniques, the results will be analyzed as presented in the next section.

3. Results and Discussion

After milling the powders, the above techniques will be used to analyze the sample's characteristics. We will present and discuss each method's results separately.

3.1 XRD Results

By exposing the milled powders to x-rays, the obtained patterns after selected milling times for the FeNi alloy and pure Fe are illustrated in Fig. 2(a) and (b), respectively.

The starting powders show only α -Fe and γ -Ni peaks (not shown in the present paper). With increasing milling time, distinct peaks at specific angles are observed, and with a decrease in their intensities, the fundamental bcc and fcc peaks become extended. For nanocrystalline Fe₅₀Ni₅₀, all of the Fe peaks have disappeared after 8h milling; however, for pure Fe, all reflection peaks of the spectrum corresponding to α -Fe bcc can be distinguished.

The Fe peaks disappearing in Fig. 2(a) may be justified by the dissolution of the smaller Fe atoms in the fcc lattice and the formation of a single phase γ -FeNi, while the diffraction peaks broaden in the pure Fe (Fig. 2b) with increasing milling time indicating a continuous decrease in the grain sizes and the introduction of lattice strain.

The γ -FeNi and α -FeNi phases are characterized by distinct crystal structures: body-centered cubic (bcc) and face-centered cubic (fcc), respectively. The bcc structure is distinguished by atoms positioned at each corner of a cube and a single atom situated at the center of the cube. Conversely, while the fcc structure also features atoms at the cube's corners, it uniquely possesses additional atoms at the centers of all the cube's faces. In (Ref 33), mixture γ -FeNi and α -FeNi phases formation has been confirmed using Pulverisette 7 planetary ball mill processing, using AGO-2U-type planetary ball mill (Ref 34), using the same SPEX 8000 D mixer/mill with a ball-to-sample weight ratio of 9 to 1 (Ref 35), planetary ball mill processing with 10 h (Ref 34), and by evaporation–condensation with a crystallite size around 45 nm (Ref 36).

The evolution of crystallite size *D* and lattice strain ϵ for nanocrystalline FeNi and pure Fe powders as a function of milling time are illustrated in Fig. 3. Figure 4 illustrates the variation of lattice parameter with increasing milling time for nanocrystalline Fe₅₀Ni₅₀ and pure Fe powders.

The comparison was done for milling times varied between 0.5 and 24 h. A reduction of the crystallite sizes (from *D* = 22 nm to 14 nm for Fe₅₀Ni₅₀ and *D* = 54 nm to 20 nm for pure Fe) was accompanied by an increase in the lattice internal strain level ϵ (increase from 0.40 to 0.65 % for FeNi alloy and 0.31 % to 0.73 % when the milling time was up to 32 h for pure Fe).

For further confirmation, we illustrate our results with those reported in the old works in Table 2.

As previously mentioned, the milling process gradually alters the Fe₅₀Ni₅₀ powder's structure by deforming the internal network, introducing atomic disorder, and creating solid solutions with an increase in lattice parameters from 0.351 nm to 0.359 nm during the first eight hours of milling. For pure

Table 1 Experimental test parameters

Studied powder	Fe	FeNi
Purity of powder	99.99%	99.99% for Fe and 99.98% for Ni
Milled composition	100% of Fe (3 g)	50% of Fe (3 g) and 50% of Ni (3 g)
Milling cycle duration	30 min	30 min
Number of cycles	64	48
Pause between milling cycles	15 min	15 min
Anticathode of the lamp for XRD analysis	Cu-K $\lambda = 1.54056$ A	Co $\lambda = 1.54056$ A
SEM and FE-SEM tests	Applied	Applied
Mössbauer test	Applied	Not applied
VSM analysis	Applied	Not applied

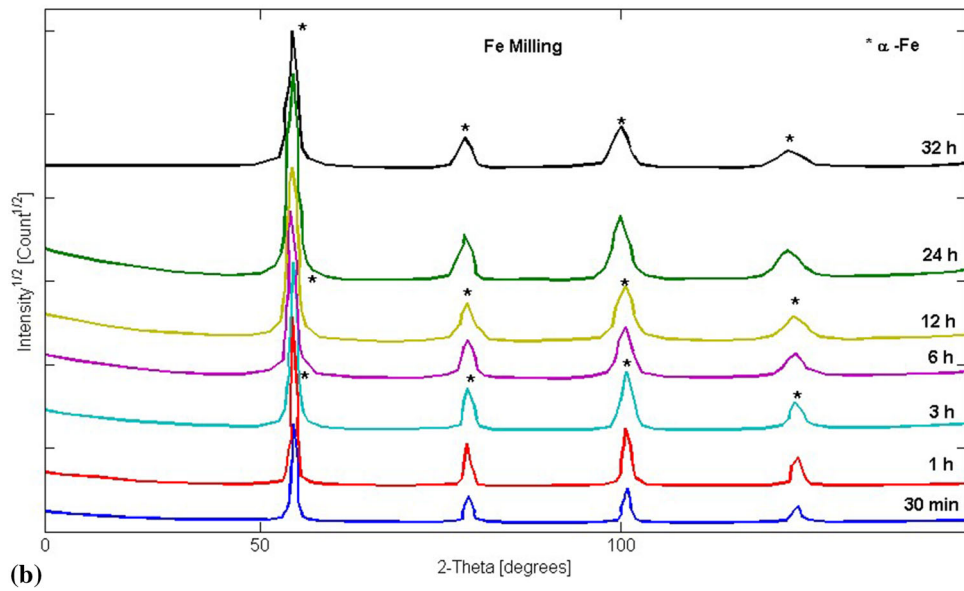
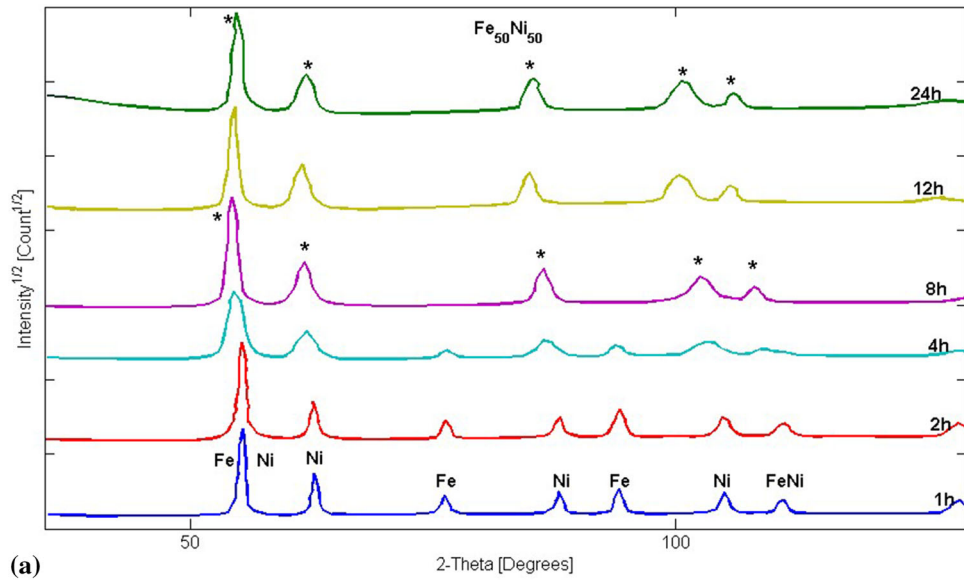


Fig. 2 X-ray diffraction patterns synthesized for various milling times: (a) nanocrystalline Fe₅₀Ni₅₀ and (b) nanocrystalline Fe

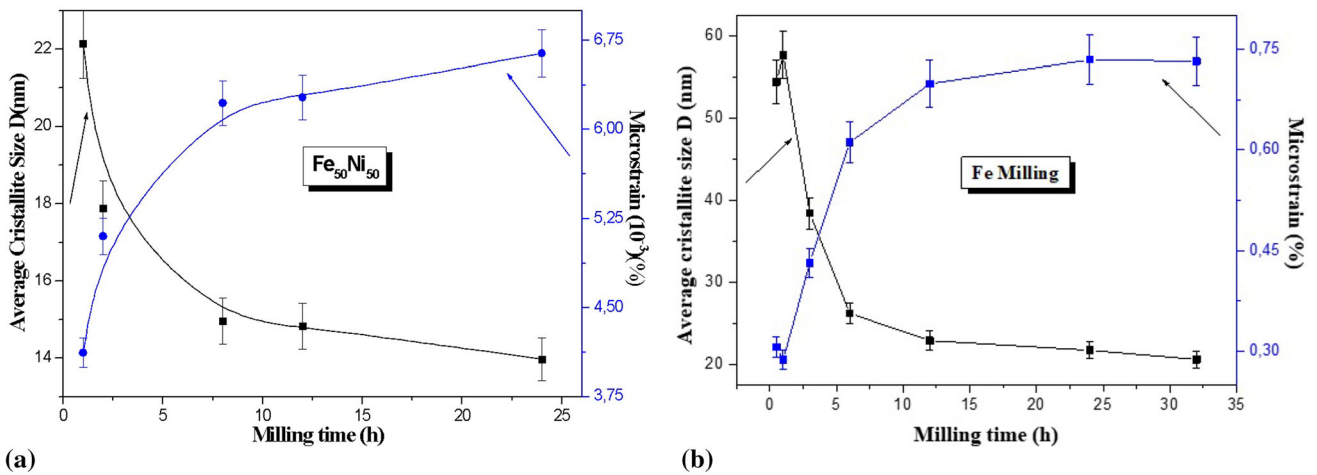


Fig. 3 Crystallite size and microstrain as a function of milling times for: (a) Fe₅₀Ni₅₀ and (b) pure Fe powders

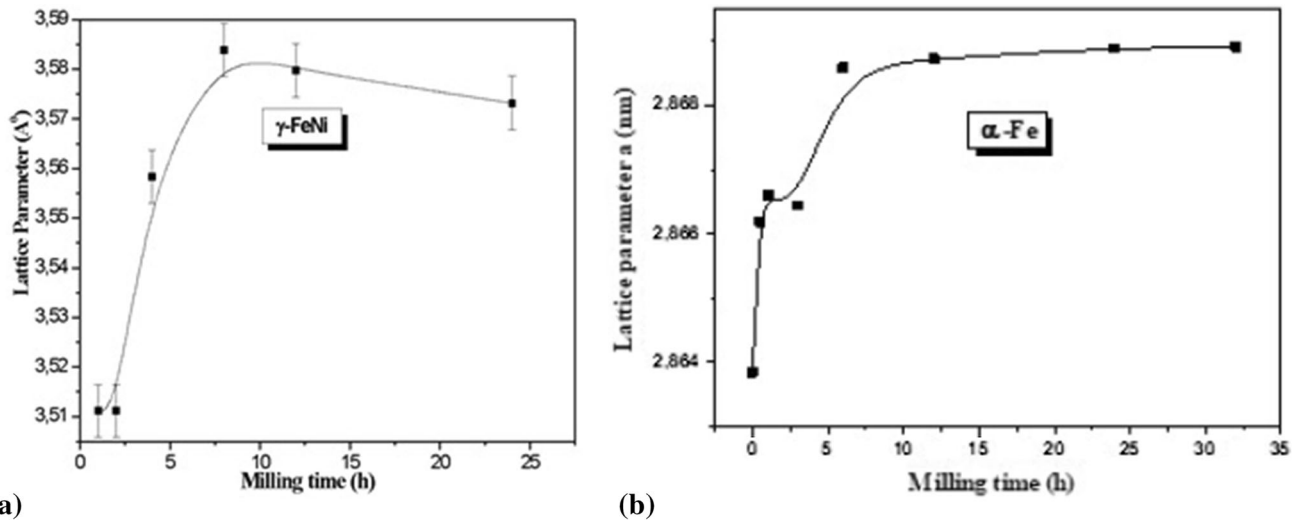


Fig. 4 Lattice parameter for various milling times of: (a) γ (fcc) and (b) α (bcc) for taenite alloy and pure Fe powders, respectively

Table 2 Comparison of crystallite size and lattice internal strain level values with estimated errors

References	Composition	Crystallite size D, nm	Lattice internal strain level ϵ , %	Milling time, h	Error in crystallite size, %	Error in lattice strain level, %
Our results		14	0.65	24		
Djekkoun et al. (Ref 33)		5	0.021	322	64.28	96.76
Pekala et al. (Ref 37)	FeNi	10	0.46	40	28.57	29.23
Jartych et al. (Ref 38)		9	0.47	400 ¹	35.71	27.69
Hamzaoui et al. (Ref 39)		10	0.69	96 ¹	28.57	6.15
Our results		20	0.73	32		
Borner et al. (Ref 40)		20	...	44	0	...
Malow et al. (Ref 41)	Fe	20	...	24	0	...
Del Bianco et al. (Ref 42)		10	...	32	50	...

¹Low-energy milling

Fe, in the same time frame, the lattice parameter has risen from 0.2864 nm to 0.2868 nm and becomes relatively stable after 12 h. Comparing these results with those reported in (Ref 43) and (Ref 36), we found a good agreement, although they applied 50 h of milling to Fe₅₀Ni₅₀ and Fe powder with a high compaction unit, respectively.

3.2 SEM and FE-SEM Results

As a second analysis, electron microscopy techniques have been used to characterize nanocrystalline Fe₅₀Ni₅₀ and

nanocrystalline Fe. So, SEM and FE-SEM have been used to determine powder morphology and particle size for the studied taenite and iron powders. The Fe₅₀Ni₅₀ alloy results are illustrated in Fig. 5 and 6.

The pure Fe results are presented for 24 and 32 h of milling only in Fig. 7.

The results clearly show the change of the powders morphologies during the mechanical alloying stages, where the particles are flattened under the force of the plastic deformation caused by the compressive forces induced during contacts between balls/powder/balls.

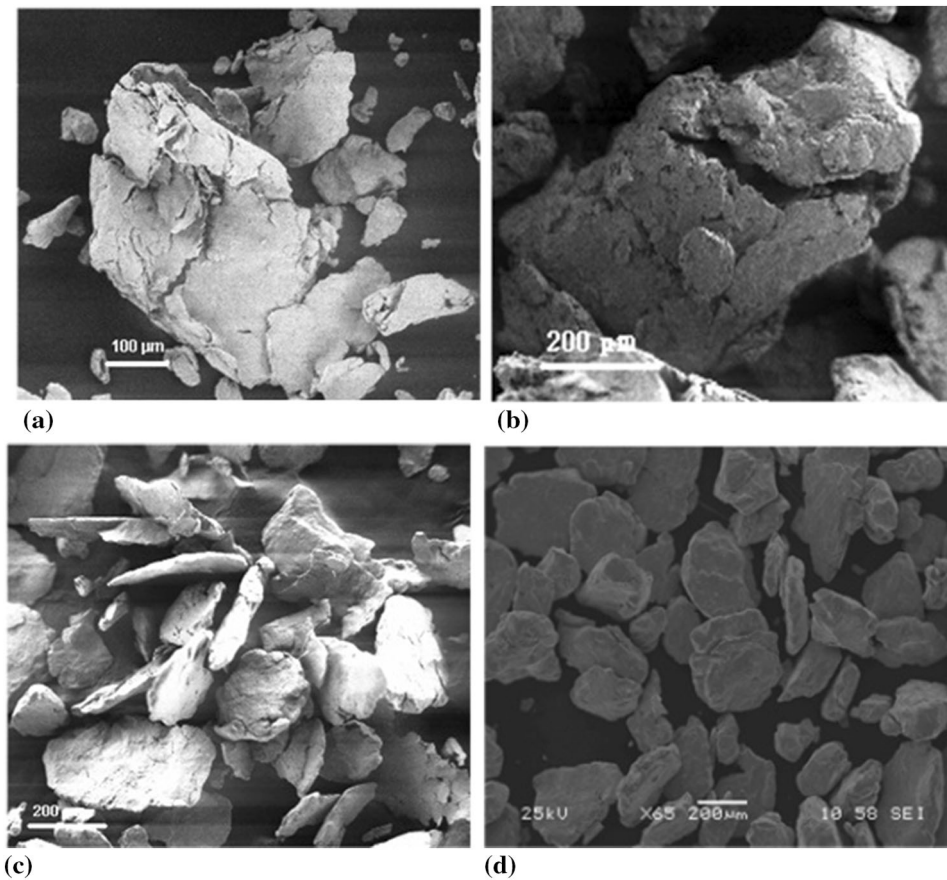


Fig. 5 SEM results for FeNi alloy results after different milling times: (a) after 1 h, (b) after 4 h, (c) after 8 h, and (d) after 12 h

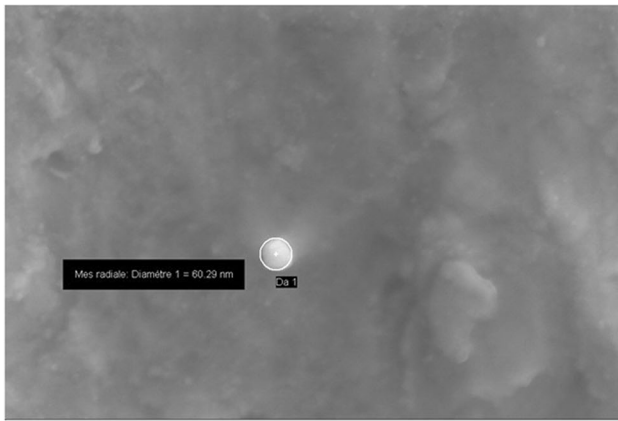
To more investigate cold melting impact, the powder has been visualized in the order of hundreds of micrometers. After two cycles of mechanical alloying (each cycle of 30min duration), the SEM results show that under the pressure of the balls, FeNi alloy particles are agglomerated and several sizes have been identified in this transient period. So, the changes in this step are remarkable (Fig. 5a). The FE-SEM image (Fig. 6a) shows the appearance of the crystallites with a diameter of about 60 nm approximately. After eight cycles of mechanical alloying, the morphological structure of the taenite alloy changes, where remarkable fracture and cold welding of particles are observed in Fig. 5(b) which purely are caused by local inner stress during subsequent milling cycles and without adding any reagent, and the crystallite size is approximately 46.89 nm as shown by the FE-SEM image in Fig. 6(b). After 8 h of milling and with the creation of fcc phase for the FeNi alloy, the morphological structure of the particles changes into a flake or platelet shape as shown in Fig. 5(c) under the pressure of balls/powder/balls contacts. Some of these particles present a superposed layers of Ni and Fe layers with sizes of 33 nm, typical of materials prepared by mechanical alloying for ductile or brittle elements as indicated by Otmani et al. (Ref 44). Micrometer aggregates of FeNi nanopowder particles are

formed during milling. The crystalline size is reduced to 33.49 nm as shown in the FE-SEM image in Fig. 6(d). With 12 h of milling, the powder particles become finer than the above ones (Fig. 5d). The complete transformation is achieved after 24 h of milling, confirmed with the other used techniques.

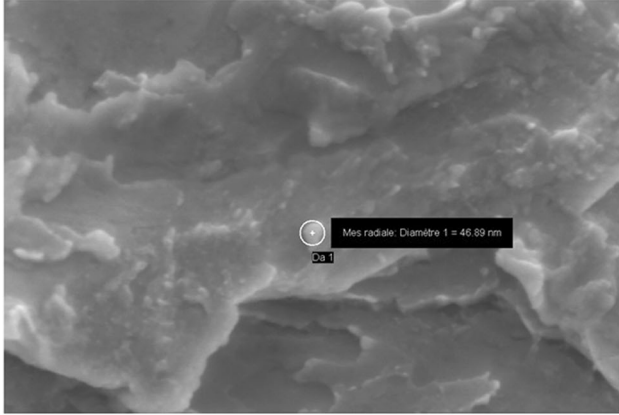
For the pure Fe powder, two steps during the milling have been examined which are, respectively, after 24 h and 32 h. The SEM results reveal that the Fe powder became finer when increasing milling time as shown by the difference between particles sizes shown in Fig. 7(a) and (b). The FE-SEM illustrates that after 24 h, the particle sizes are of 13 nm (Fig. 7c), but an increase to 15 nm (Fig. 7d) is noted. Since the contact balls/powder/balls leads to intensive fracture between particles, the waited results were the decrease in the particles sizes, but a cold welding appears with maintenance of fcc phase in the particles leading to an increase in the sizes compared to FeNi where phase change appears.

3.3 Mössbauer Results

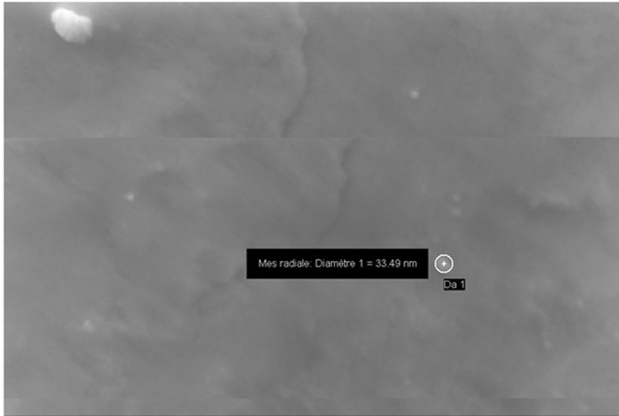
To study magnetic structure of FeNi, Mössbauer spectroscopy has been applied for the milled powders. The room-



(a) $D = 60.29 \text{ nm}$



(b) $D = 49.69 \text{ nm}$



(c) $D = 33.49 \text{ nm}$

Fig. 6 FE-SEM results for FeNi alloy results after different milling times: (a) after 1 h, (b) after 4 h, and (c) after 8 h

temperature Mössbauer spectra and their corresponding HFD for different milling times are shown in Fig. 8.

In the initial phase (the sample was unmilled), the spectrum shows the presence of a typical sextet. After 2 h of milling, the spectra were fitted using a magnetic HFD, and a mean

hyperfine field $\langle B_{hf} \rangle$ is equal to 33 T which corresponds to the α -Fe presence in the starting FeNi powder milling. When the samples are milled for 8 and 24 h, the shape of the spectra changes with a broadening of the spectral lines in relation to α -iron. This broadening arises due to the alloying progress, the grain size reduction, and the increasing microstrains. It can be attributed to FeNi γ phase (Ni-rich taenite). It should be noted that the hyperfine field $\langle B_{hf} \rangle$ is reduced to 32 and 30, respectively.

Identical observations have been made for milling going from 2 to 33 h (Ref 45), where the hyperfine field $\langle B_{hf} \rangle$ is 33, 32, 31, and 29T, respectively, for 0, 2, 8, and 24 h of milling. Freeland et al. (Ref 46) have obtained hyperfine field of $\sim 30 \text{ T}$ (at 13 K) for γ (fcc) FeNi thin film alloys, while Lima et al. (Ref 47) found that $B_{hf} = 29.5 \text{ T}$ for nanostructured Fe₅₀Ni₅₀ alloy prepared by chemical reduction.

3.4 VSM results

The magnetization measurements for Fe₅₀Ni₅₀ alloys were taken using Vibrating Sample Magnetometer (VSM) at room temperature with an applied magnetic field of 16 kOe. Magnetic Hysteresis loops of nanocrystalline Fe₅₀Ni₅₀ samples obtained with several milling times are shown in Fig. 9.

The results show that the milling time has a direct impact on the Hysteresis loops, where the change of the phase has an impact on the remanent field and saturation induction, but the shape is similar for all milling times. For further illustration of the principal changes due to the milling, the coercive and saturation magnetization variations as function of milling time are illustrated in Fig. 10, and the remnant magnetization and squareness ratio (Ref 48) in function of milling time are presented in Fig. 11.

We note that in the beginning of milling, the FeNi powder morphology changes, and these changes were characterized by particles fracture, and Hysteresis cycle was obtained, different to the one obtained at the beginning. After 8 h of milling, due to the presence of superposed layers of Ni and Fe, the Hysteresis loops have been changed slightly and become, after that, similar to the ones obtained after 4 h of milling.

In some Ref 49, 50, the M-H characteristics have been used to estimate the effect of magnetocrystalline anisotropy and to determine coercitif field with a considerable applied field of 7T.

The results presented in Fig. 10 show two distinct phases: in the first 2 h of milling, where saturation magnetization decreases significantly and coercivity increases, and the rest of milling time, where saturation magnetization increases and coercivity decreases.

The remanent magnetization and squareness ratio changes of the Fe₅₀Ni₅₀ alloy during 12 h of milling are presented in Fig. 11.

The results shown in Fig. 11 illustrate that the remnant magnetization of the Fe₅₀Ni₅₀ alloy increases after 2 h of milling to 0.3 emu. This increase is caused by the morphological change of the taenite's nanoparticles because of fractures and cold welding. After that, the both parameters values

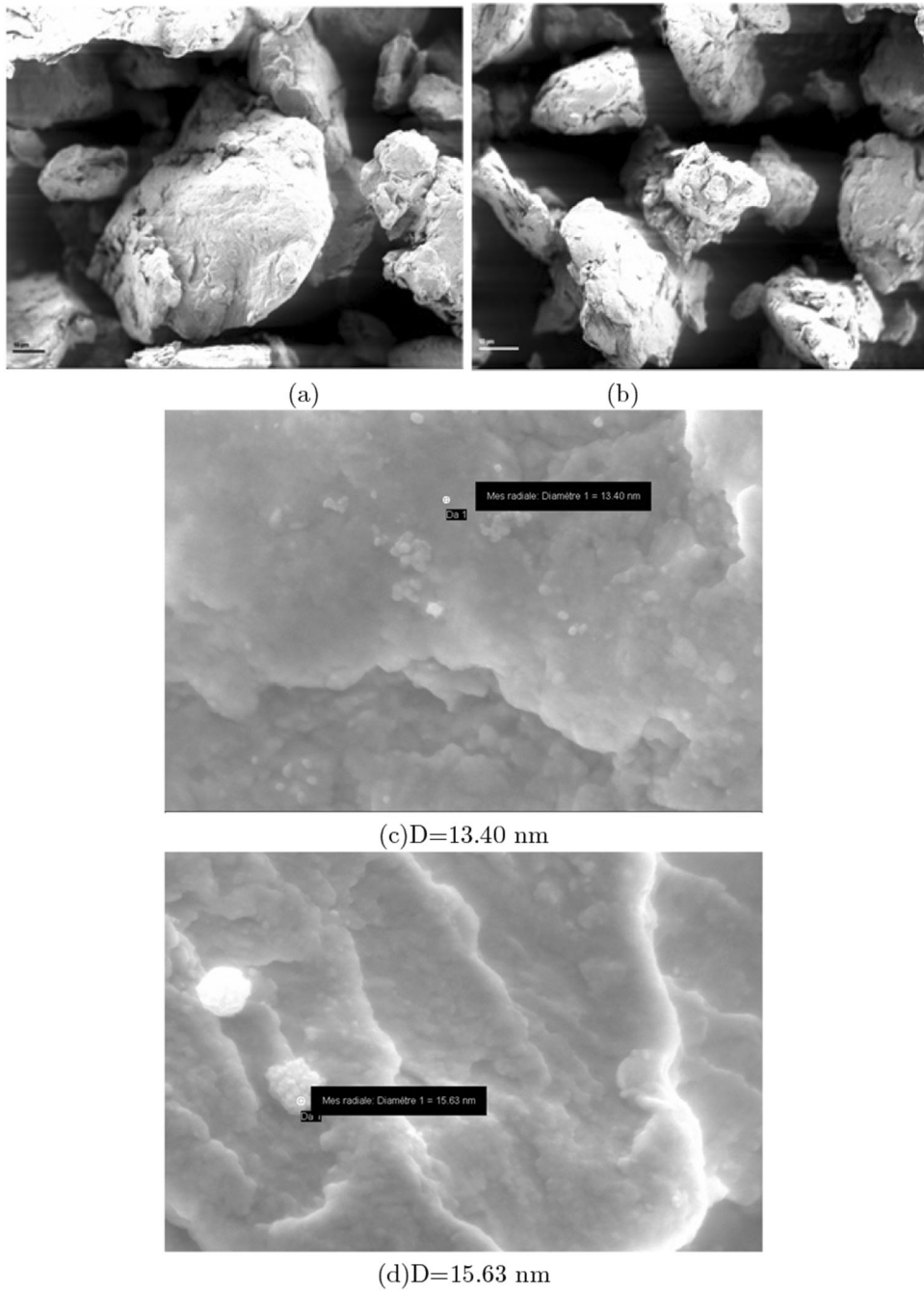


Fig. 7 Nanocrystalline Fe results after different milling times: (a) SEM after 24 h, (b) SEM after 32 h, (c) FE-SEM after 24 h, and (d) FE-SEM after 32 h

decrease preparing for the new phase after these hours where the coercivity decreases and the saturation magnetization remains constant and increases after the fourth hour as shown above in Fig. 10.

In the same time, the squareness ratio is characterized approximately by the same changes, where it increases to 0.047 in the first two hours of milling and then it decreases back to the initial value. So, the changes during milling in squareness ratio characterizing Hysteresis cycle are affecting only the milled

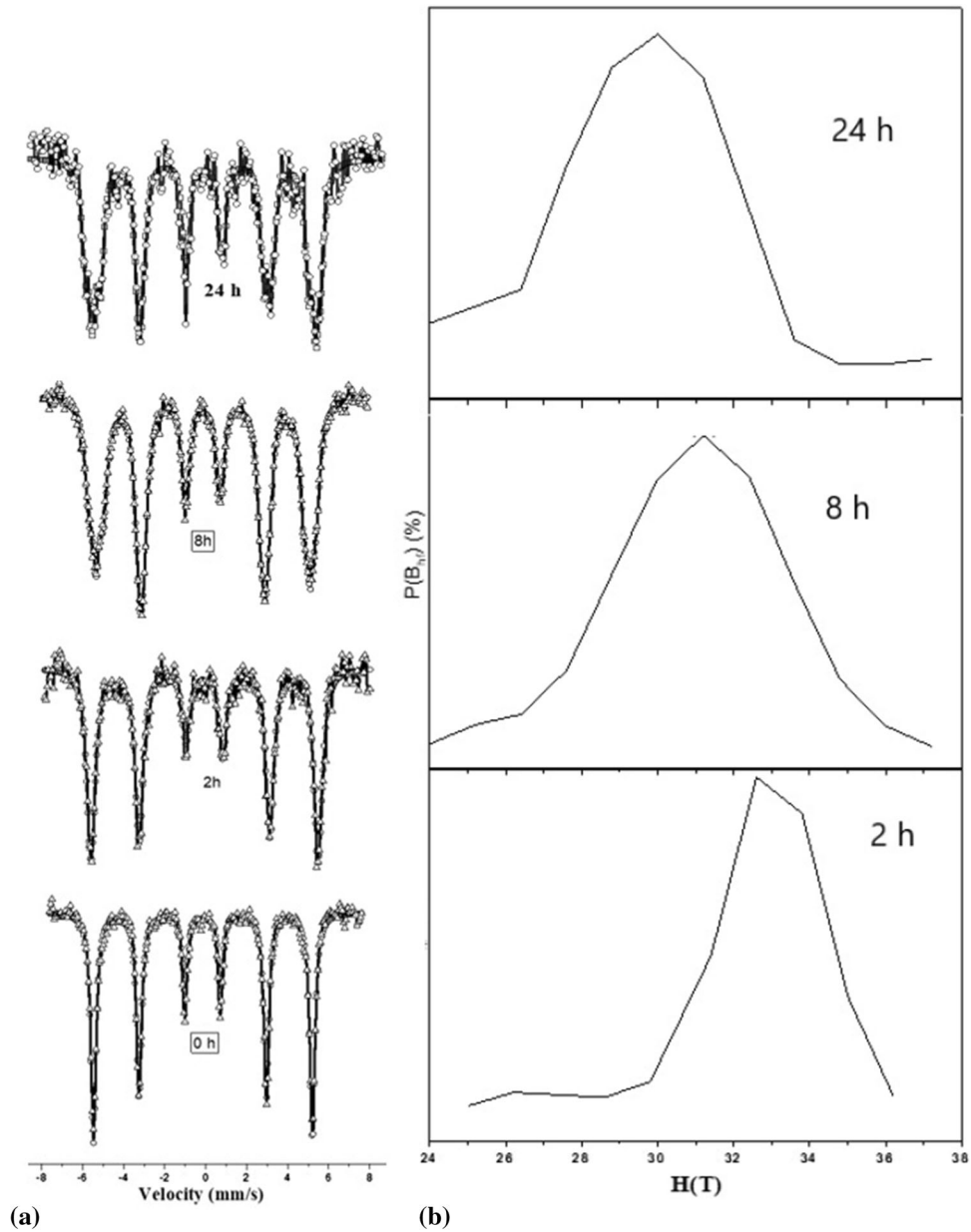


Fig. 8 Room-temperature Mössbauer results for FeNi alloy: (a) Mössbauer spectra and (b) hyperfine field distribution

powder during two hours. The magnetic parameters after that are amortized.

We note that the decrease in coercivity value may be due to the anisotropy field decrease, which leads to domain wall energy reduction (Ref 43, 51, 52).

By using these results and the equations mentioned in (Ref 53, 54), we estimate that uniaxial magnetocrystalline anisotropy is $K_u = 6.06$.

According to Morrish Law which uses uniaxial magnetocrystalline anisotropy to determine anisotropic field (Ref 55):

$$H_a = \frac{2K_u}{\mu_0 M_s} \quad (\text{Eq 1})$$

where H_a is anisotropic field, M_s is magnetization saturation, μ_0 is air magnetic permeability, and K_u is uniaxial magnetocrystalline anisotropy, and the anisotropic field after 12 h of milling is 1478.385 G. Furthermore, with taking into consideration molecular weight of FeNi alloy Mw (114.5384 g/mol) and the development based on the works (Ref 56-58) to determine

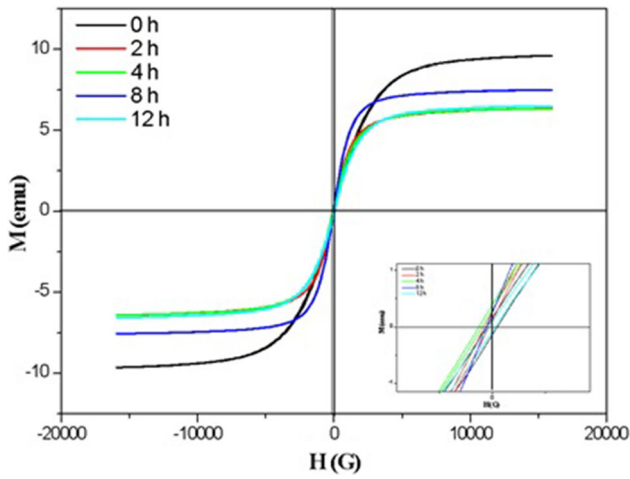


Fig. 9 Hysteresis loops for milled FeNi nanostructured powder with various milling times

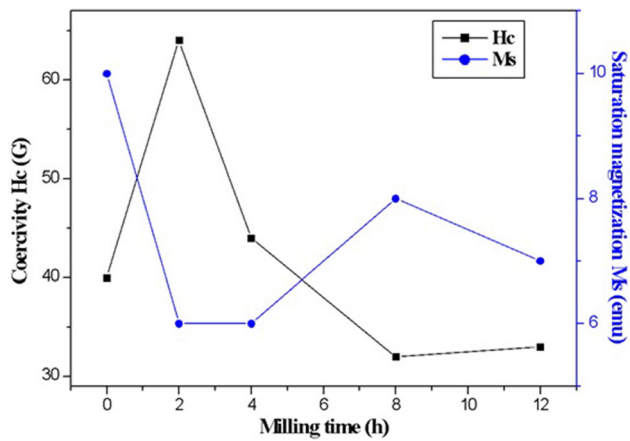


Fig. 10 Variation of FeNi saturation magnetization (M_s) and coercivity (H_c) as function of milling time

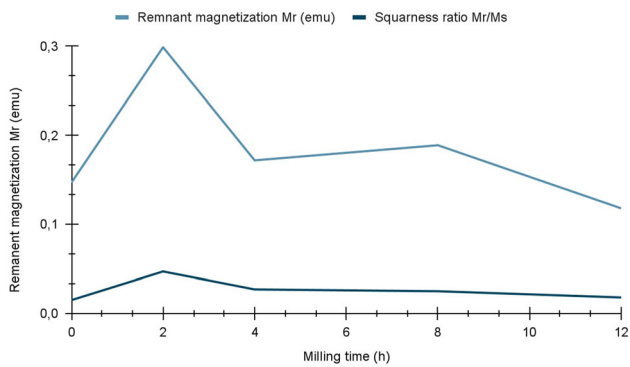


Fig. 11 Variation of remnant magnetization and squareness ratio for FeNi as function of milling time

magnetic moment in Bohr magneton (B), the value obtained is 0.1338.

The next table illustrates a comparative analysis between Fe and FeNi results (Table 3).

4. Conclusion

The characteristics of nanocrystal FeNi and Fe powder prepared with mechanical alloying have been studied in this paper. The powders of FeNi and Fe have been milled for 24 and 32 h, respectively. During the milling, the microstructure, morphology, and magnetic properties of powders samples have been analyzed using XRD, SEM, and FE-SEM. The results show that the nanocrystal FeNi powder:

1. The γ and α phases of FeNi are characterized by bcc and fcc, respectively, where this is later identified after 8h milling;
2. In the beginning of milling, different sizes of the particles are identified which attains 60.29 nm, and after the milling time increases, the particles sizes are harmonized to approximately 14 nm with 0.65 % internal strain;
3. Morphological structure of the powder changes with the increase in milling time, where a remarkable difference is appearing in the beginning, and the particles size becomes practically the same (33 nm, reported by FE-SEM) at the end of milling;
4. The Mössbauer spectra contain the γ (FCC) phase with a hyperfine field B_{hf} value of 32, 31, and 29 T, respectively for 2 h, 8 h, and 24 h milling times.

The results for pure Fe powder show that:

1. The α peaks appearing in the XRD results prove the unique structure, bcc, whatever the milling time;
2. The particles sizes have been reduced to 20 nm and internal strain about 0.73 %;
3. With the increase in the milling time, the Fe particles becomes finer (13 nm) because of the intensive fracture;
4. Cold welding appearance during milling, causing slight increase (attains 10 %) in the particles sizes.

Vibrating sample magnetometer has been applied for FeNi alloy where coercivity decreases from 39.48 to 32.85 G. After 8 h and because of anisotropy field decrease leading to a loss in domain wall energy, the saturation magnetization increases to 7.53 emu. At the end of milling, it becomes 6.5 emu. By analyzing VSM results for 12 h of milling, the uniaxial magnetocrystalline anisotropy is $K_u = 6.06$, the anisotropic field is 1478.385 G, and the magnetic moment in Bohr magneton is 0.1338.

With the parameters studied for the FeNi alloy, showing the milling contribution in the change of the crystallite size and microstrain, where the Fe and Ni particles become layered

Table 3 Comparison between Fe and FeNi

Powder	Fe	FeNi
Methodology of analysis	XRD SEM FE-SEM	XRD SEM FE-SEM Mössbauer spectroscopy VSM
Milling time	32 h	24 h
Phases appearing	Bcc	Bcc an fcc
Crystallite size	14 nm	20 nm
Mössbauer analysis	...	Mean field of 33 T
Coercivity after 12 h of milling	...	33 G
Saturation magnetization after 12 h of milling	...	7 emu
Applications	Metallurgical processes to control iron density	Magnetic circuits with high frequencies

under the pressure of milling balls, the magnetocrystalline anisotropy show that such nanomaterial is suitable for a range of applications that require a strong magnetic response.

Acknowledgments

This work was supported by Laboratoire de Magnetisme et de Spectroscopie des Solides, Badji Mokhtar University, Annaba, Algeria.

Author Contributions

N. Boudinar, A. Djekoun, and B. Bouzabata contributed to experimental tests. N. Boudinar and S. Chiheb Paper contributed to redaction and results discussions. N. Nedjah and N. Arabi Magnetics contributed to characteristics.

References

- Nieman, G., J. Weertman, and R. Siegel. 1990. Tensile strength and creep properties of nanocrystalline palladium. *Scr. Metall. Mater.* 24: 145–150
- Patelli, N., F. Cugini, D. Wang, S. Sanna, M. Solzi, H. Hahn, and L. Pasquini. 2022. Structure and magnetic properties of Fe-Co alloy nanoparticles synthesized by pulsed-laser inert gas condensation. *J. Alloy. Compd.* 890: 161863
- Cheung, C., G. Palumbo, and U. Erb. 1994. Synthesis of nanocrystalline permalloy by electrodeposition. *Scr. Metall. Mater.* 31: 735–740
- Cesiulis, H., N. Tsytaru, E.J. Podlaha, D. Li, and J. Sort. 2019. Electrodeposition of iron-group alloys into nanostructured oxide membranes: synthetic challenges and properties. *Curr. Nanosci.* 15: 84–99
- Makino, A., A. Inoue, and T. Masumoto. 1995. Nanocrystalline soft magnetic Fe-m-b (m= Zr, Hf, Nb) alloys produced by crystallization of amorphous phase (overview). *Mater. Trans., JIM* 36: 924–938
- Wang, F., A. Inoue, F. Kong, S. Zhu, E. Shalaan, F. Al-Marzouki, W. Botta, C. Kiminami, Y.P. Ivanov, and A. Greer. 2019. Formation, stability and ultrahigh strength of novel nanostructured alloys by partial crystallization of high-entropy (Fe_{0.25}Co_{0.25}Ni_{0.25}Cr_{0.125}Mo_{0.125}) amorphous phase. *Acta Materialia* 170: 50–61
- Hahn, H. and R. Averback. 1990. The production of nanocrystalline powders by magnetron sputtering. *J. Appl. Phys.* 67: 1113–1115
- Wang, J.-P. 2008. FePt magnetic nanoparticles and their assembly for future magnetic media. *Proc. IEEE* 96: 1847–1863

- Ar, Y. and O. Drbohlav. 1995. Thermodynamics and kinetics of nanostructure formation in soft-magnetic nanocrystalline alloys (overview). *Mater. Trans., JIM* 36: 896–902
- Suryanarayana, C., A.A. Al-Joubori, and Z. Wang. 2022. Nanostructured materials and nanocomposites by mechanical alloying: An overview. *Met. Mater. Int.* 28: 41–53
- Meng, B., J. Wang, M. Chen, S. Zhu, and F. Wang. 2023. Study on the oxidation behavior of a novel thermal barrier coating system using the nanocrystalline coating as bonding coating on the single-crystal superalloy. *Corros. Sci.* 225: 111591
- Zhao, Y., K. Liu, H. Zhang, X. Tian, Q. Jiang, V. Murugadoss, and H. Hou. 2022. Dislocation motion in plastic deformation of nano polycrystalline metal materials: a phase field crystal method study. *Adv. Comp. Hybrid Mater.* 5(3): 2546–2556
- Suryanarayana, C. 2022. Mechanical alloying: a critical review. *Mater. Res. Lett.* 10: 619–647
- Suryanarayana, C. 2019. Mechanical alloying: a novel technique to synthesize advanced materials, Research, p 1-17
- Zhang, C. and I. Zhitomirsky. 2022. Influence of high energy ball milling and dispersant on capacitive properties of Fe₂O₃-carbon nanotube composites. *J. Compt. Sci.* 6: 177
- Liu, J., C. Li, S. Zhang, J. Feng, P. Zhang, and L. Zhou. 2017. Phase transition mechanism of Fe_{1.1}Se_{0.5}Te_{0.5} fabricated by high-energy ball milling aided sintering method. *IEEE Trans. Appl. Supercond.* 27: 1–5
- Kurichenko, V.L., D.Y. Karpenkov, A.Y. Karpenkov, M.B. Lyakhova, and V.V. Khovaylo. 2019. Synthesis of FeNi tetraetaenite phase by means of chemical precipitation. *J. Magn. Magn. Mater.* 470: 33–37
- Freire, T., R. Freire, M. Franco, E. Lopez, R. de Oliveira, J. Denardin, F. Oliveira, I. Vasconcelos, P. Casciano, P. de Lima-Neto, et al. 2022. Magnetic Fe_m (m= Ag Co, Cu, and Ni) nanocrystals as electrocatalysts for hydrogen evolution reaction. *Mater. Today Sustain.* 18: 100150
- Panigrahi, M. and B. Avar. 2021. Influence of mechanical alloying on structural, thermal, and magnetic properties of Fe₅₀Ni₁₀Co₁₀Ti₁₀B₂₀ high entropy soft magnetic alloy. *J. Mater. Sci.-Mater. Electr.* 32(16): 21124–21134
- Xie, J., Y. Chen, H. Wang, T. Zhang, M. Zheng, S. Wang, L. Yin, J. Shen, and J.P. Oliveira. 2024. Phase transformation mechanisms of NiTi shape memory alloy during electromagnetic pulse welding of Al/NiTi dissimilar joints. *Mater. Sci. Eng., A* 893: 146119
- Long, X., K. Chong, Y. Su, C. Chang, and L. Zhao. 2023. Meso-scale low-cycle fatigue damage of polycrystalline nickel-based alloy by crystal plasticity finite element method. *Int. J. Fatigue* 175: 107778
- Mushnikov, N., A. Popov, V. Gaviko, A. Protasov, N. Kleinerman, O. Golovnya, and S. Naumov. 2022. Peculiarities of phase diagram of Fe-Ni system at Ni concentrations 0-20 %. *Acta Mater.* 240: 18330
- Sharma, M.K., A. Kumar, K. Kumari, S.-J. Park, N. Yadav, S.-H. Huh, and B.-H. Koo. 2023. Evidence of hysteresis free ferromagnetic nature and significant magnetocaloric parameters in FeNi binary alloy. *Magnetochemistry* 9(1): 8
- Rodriguez, V.P., C. Rojas-Ayala, J.M. Medina, P.P. Cabrera, J. Quispe-Marcatoma, C. Landauro, J.R. Tapia, E. Baggio-Saitovitch, and E. Passamani. 2019. Fe₅₀Ni₅₀ synthesized by high energy ball milling: a

- systematic study using X-ray diffraction, exafs and Mössbauer methods. *Mater. Charact.* 149: 249–254
25. Pena Rodriguez, V., J. Medina Medina, C. Rojas-Ayala, P. Paucar Cabrera, C. Landauro, J. Quispe-Marcotoma, J. Rojas Tapia, E. Baggio Saitovitch, and E. Passamani. 2021. Nanostructured FeNiZrB powders synthesized by high-energy ball milling: structural and hyperfine characterizations. *Hyperf. Interact.* 242: 1–16
 26. Panigrahi, M. and B. Avar. 2021. Development of microstructural and magnetic properties of Co₅₀Si₅₀ alloy powders during mechanical alloying approach. *Appl. Phys. A-Mater. Sci. Process.* 127(12): 1–10
 27. Gaylan, Y., B. Avar, M. Panigrahi, B. Aygün, and A. Karabulut. 2021. Effect of the B₄C content on microstructure, microhardness, corrosion, and neutron shielding properties of Al-B₄C composites. *Ceram. Int.* 49(3): 5479–5488
 28. Boudinar, N., A. Djekoun, A. Otmani, B. Bouzabata, J. Greneche, and K. Tiabi. 2015. Formation of nanocrystalline Fe-Ni alloys powders by mechanical alloying method. *Adv. Mater. Process. Technol.* 1: 288–293
 29. Suryanarayana, C. 2001. Mechanical alloying and milling. *Progr. Mater. Sci.* 46(1): 184
 30. Suryanarayana, C. and F. Froes. 1992. Light metals synthesis by mechanical alloying. *Mater. Sci. Forum* 88: 445–452
 31. Koch, C. 1993. The synthesis and structure of nanocrystalline materials produced by mechanical attrition: a review. *Nanostruct. Mater.* 2: 109–129
 32. L. Lutterotti, Maud cpd newsletter, IUCr, 2000, 24
 33. Djekoun, A., A. Otmani, B. Bouzabata, L. Bechiri, N. Randrianantoandro, and J. Greneche. 2006. Synthesis and characterization of high-energy ball milled nanostructured Fe₅₀Ni₅₀. *Catal. Today* 113: 235–239
 34. Baldokhin, Y.V., V. Tcherdyntsev, S. Kaloshkin, G. Kochetov, and Y.A. Pustov. 1999. Transformations and fine magnetic structure of mechanically alloyed Fe-Ni alloys. *J. Magn. Magn. Mater.* 203: 313–315
 35. Abdu, Y., T. Ericsson, and H. Annersten. 2004. Coexisting antiferromagnetism and ferromagnetism in mechanically alloyed Fe-rich Fe-Ni alloys: implications regarding the Fe-Ni phase diagram below 400 °C. *J. Magn. Magn. Mater.* 280: 395–403
 36. Djekoun, A., B. Bouzabata, S. Alleg, J. Greneche, and A. Otmani. 1998. Synthesis and morphological characterization of nanocrystalline powders obtained by a gas condensation method. *Annales de Chimie Science des Materiaux* 23: 557–562
 37. Pekala, M., D. Oleszak, E. Jartych, and J. Zurawicz. 1999. Structural and magnetic study of mechanically alloyed Fe-Ni. *Nanostruct. Mater.* 11: 789–796
 38. Jartych, E., J.K. Zurawicz, D. Oleszak, and M. la Peka. 2000. X-ray diffraction, magnetization and Mössbauer studies of nanocrystalline Fe-Ni alloys prepared by low- and high-energy ball milling. *J. Magnet. Mater.* 208: 221–230
 39. Hamzaoui, R., O. Elkedim, E. Gaffet, and J.-M. Greneche. 2006. Structure, magnetic and Mössbauer studies of mechanically alloyed Fe-20 % Ni powders. *J. Alloy. Compd.* 417: 32–38
 40. Eckert, J. and I. Bormer. 1997. Nanostructure formation and properties of ballmilled intermetallic compound. *Mater. Sci. Eng., A* 239: 619–624
 41. Malow, T. and C. Koch. 1997. Grain growth in nanocrystalline iron prepared by mechanical attrition. *Acta Mater.* 45: 2177–2186
 42. Del Bianco, L., C. Ballesteros, J. Rojo, and A. Hernando. 1998. Magnetically ordered fcc structure at the relaxed grain boundaries of pure nanocrystalline Fe. *Phys. Rev. Lett.* 81: 4500
 43. Guittoum, A., A. Layadi, A. Bourzami, H. Tafat, N. Souami, S. Boutarfaia, and D. Lacour. 2008. X-ray diffraction, microstructure, Mössbauer and magnetization studies of nanostructured Fe₅₀Ni₅₀ alloy prepared by mechanical alloying. *J. Magn. Magn. Mater.* 320: 1385–1392
 44. Djekoun, A., B. Bouzabata, A. Otmani, and J. Greneche. 2004. X-ray diffraction and Mössbauer studies of nanocrystalline Fe Ni alloys prepared by mechanical alloying. *Catal. Today* 89: 319–323
 45. Djekoun, A., B. Bouzabata, S. Alleg, J.M. Greneche, and A. Otmani. 1998. Synthesis and morphological characterization of nanocrystalline powders obtained by a gas condensation method. *Annales de Chimie Science des Materiaux* 23: 557–562
 46. Freeland, J., I. Grigorov, and J. Walker. 1998. Magnetic phase transition in epitaxial Ni_{1-x}Fe_x alloy thin films. *Phys. Rev. B* 57: 80
 47. Lima, E., Jr., V. Drago, R. Bolsoni, and P.F. Fichtner. 2003. Nanostructured Fe₅₀Ni₅₀ alloy formed by chemical reduction. *Solid State Commun.* 125: 265–270
 48. Skomski, R. 2008. *Simple models of magnetism*. Oxford: Oxford University Press
 49. Chandekar, K.V. and S.P. Yadav. 2023. Comprehensive study of MFe₂O₄ (M=Co, Ni, Zn) nanostructures prepared by co-precipitation route. *J. Alloys Compd.* 960: 170838
 50. Chandekar, Kamlesh V., and K. Mohan Kant. 2018. Estimation of the spin-spin relaxation time of surfactant coated CoFe₂O₄ nanoparticles by electron paramagnetic resonance spectroscopy. *Physica E* 104: 192–205
 51. Singhal, S., T. Namgyal, S. Bansal, and K. Chandra. 2010. Effect of Zn substitution on the magnetic properties of cobalt ferrite nano particles prepared via sol-gel route. *J. Electromagn. Anal. Appl.* 10(6): 376–381
 52. Singhal, S., S. Barthwal, and K. Chandra. 2006. Xrd, magnetic and Mössbauer spectral studies of nano size aluminum substituted cobalt ferrites (CoAl_xFe_{2-x}O₄). *J. Magn. Magn. Mater.* 306: 233–240
 53. Jiles, D. 2015. *Introduction to magnetism and magnetic materials*. CRC Press
 54. Cullity, B.D. and C.D. Graham. 2011. *Introduction to magnetic materials*. Hoboken: Wiley
 55. AH. Morrish. *The physical principles of magnetism*. 2001
 56. Chandekar, K.V. and K.M. Kant. 2018. Relaxation phenomenon and relaxivity of cetrimonium bromide (CTAB) coated CoFe₂O₄ nanoparticles. *Physica B: Condensed Matter* 545: 536–548
 57. Chandekar, K.V. and K. Kant-Mohan. 2017. Effect of size and shape dependent anisotropy on superparamagnetic property of CoFe₂O₄ nanoparticles and nanoplatelets. *Physica B: Condensed Matter* 520: 152–163
 58. Chandekar, K.V., M. Shkir, T. Alshahrani, et al. 2021. One-spot fabrication and in-vivo toxicity evaluation of core-shell magnetic nanoparticles. *Mater. Sci. Eng., C* 122: 111898

Publisher's Note Springer Nature remains neutral with regard to jurisdictional claims in published maps and institutional affiliations.

Springer Nature or its licensor (e.g. a society or other partner) holds exclusive rights to this article under a publishing agreement with the author(s) or other rightsholder(s); author self-archiving of the accepted manuscript version of this article is solely governed by the terms of such publishing agreement and applicable law.